energies

MDPI

Article

Performance Simulation of Solar Trough Concentrators: Optical and Thermal Comparisons

Fei Cao *, Jiarui Pang, Xianzhe Gu, Miaomiao Wang and Yanqin Shangguan

College of Mechanical and Electrical Engineering, Hohai University, Changzhou 213022, China
* Correspondence: fcao@hhu.edu.cn

Abstract: The solar trough concentrator is used to increase the solar radiation intensity on absorbers for water heating, desalination, or power generation purposes. In this study, optical performances of four solar trough concentrators, viz. the parabolic trough concentrator (PTC), the compound parabolic concentrator (CPC), the surface uniform concentrator (SUC), and the trapezoid trough concentrator (TTC), are simulated using the Monte Carlo Ray Tracing method. Mathematical models for the solar trough concentrators are first established. The solar radiation distributions on their receivers are then simulated. The solar water heating performances using the solar trough concentrators are finally compared. The results show that, as a high-concentration ratio concentrator, the PTC can achieve the highest heat flux, but suffers from the worst uniformity on the absorber, which is only 0.32%. The CPC can generate the highest heat flux among the rest three low-concentration ratio solar trough concentrators. Compared with the PTC and the CPC, the TTC has better uniformity, but its light-receiving ratio is only 70%. The SUC is beneficial for its highest uniformity of 87.38%. Thermal analysis results show that the water temperatures inside the solar trough concentrators are directly proportional to their wall temperature, with the highest temperature rise in the PTC and the smallest temperature rise in the TTC. The solar trough concentrators' thermal deformations are positively correlated to their wall temperatures. The radial deformation of the SUC is much larger than those of other solar trough concentrators. The smallest equivalent stress is found in the SUC, which is beneficial to the long-term operation of the solar water heating system.

Keywords: solar collector; parabolic trough concentrator; compound parabolic concentrator; surface uniform concentrator; trapezoid trough concentrator; optical performance; thermal deformation

Citation: Cao, F.; Pang, J.; Gu, X.; Wang, M.; Shangguan, Y. Performance Simulation of Solar Trough Concentrators: Optical and Thermal Comparisons. *Energies* **2023**, *16*, 1673. https://doi.org/10.3390/en16041673

Academic Editor: Manolis Souliotis

Received: 6 January 2023
Revised: 31 January 2023
Accepted: 4 February 2023
Published: 7 February 2023

1. Introduction

Due to the low flux intensity, fluctuant and periodicity characteristics of solar energy, concentrators are of high importance to solar energy applications. The solar trough concentrator (STC) is one of the most developed solar concentrators. The STC has a trough shape reflector, which can focus sunlight to a line. There are many kinds of STCs reported in the literature, for example, the parabolic trough concentrator (PTC), the compound parabolic concentrator (CPC), the V-shaped trough concentrator (VTC) and the trapezoidal-shaped trough concentrator (TTC), etc. Extensive simulation and experimental studies have been reported in the literature for different STC types and their applications.

Padilla et al. conducted a one-dimensional numerical heat transfer analysis on PTC and found that the PTC has better performance for reducing heat loss [1]. Wang et al. proposed a new concept of negative heat flux region, which provides a new optimization strategy for reducing the radiant heat loss of PTC [2]. Avargani and Divband evaluated the performance of a solar water heating (SWH) system with glass-covered PTCs under different system tracking modes [3]. Bellos et al. found that the absorber geometry was one main factor influencing the PTC performance and designed a dimpled absorber tube with sine geometry which increased the heat transfer surface and the flow turbulence [4]. Freeman et al. proposed and evaluated a PTC-powered organic Rankine cycle (ORC) system

for combined heating and power applications in the UK [5]. Nafey and Sharaf designed and analyzed an ORC system with a reverse osmosis desalination process driven by solar PTC and CPC respectively [6]. Zou et al. experimentally investigated a small-sized solar PTC for SWH in cold areas [7]. Calise established a dynamic model of a solar PTC-based heating and cooling system with a double-stage LiBr-H_2O absorption chiller [8]. Coccia et al. manufactured a low-cost PTC for industrial process heat applications whose working temperature ranged from 70 to 250 °C [9]. El Fadar et al. studied an adsorption refrigeration system powered by PTC with a heat pipe [10]. Sanda et al. reviewed the modelling and simulation tools for direct steam generation (DSG) with PTCs [11]. Temiz and Dincer proposed a solar PTC-driven thermochemical hydrogen production plant with thermal energy storage and geothermal systems [12]. Sharaf et al. carried out a thermo-economic analysis of PTC-assisted MED-VC desalination processes [13]. Kabeel et al. analyzed a passive solar water desalination system with a PTC-incorporated latent heat storage medium and concluded that the daily freshwater yield with the PTCs was nearly 50% higher than that with usual solar-based still [14].

Su et al. analyzed the optical and thermal performances of a CPC and found that the absorber received solar radiation was related to the sunlight incident angle [15]. Abdullahi et al. compared the optical efficiencies of horizontal and vertical CPCs by using Monte Carlo Ray Tracing (MCRT) method and found that the performance of horizontal CPC was 15% higher than that of the vertical CPC [16]. Ustaoglu et al. evaluated the optical, thermal and radiation distribution properties of a truncated CPC with the MCRT method, and found that the optimized incident angle was 20° [17]. Waghmare and Gulhane evaluated the CPC optical performance at low reception angles to improve the overall collector performance by minimizing optical loss [18]. Xu et al. combined the CPC with a closed-end pulsating heat pipe and carried out an experimental investigation [19]. Mohan et al. proposed a solar CPC-driven system for sustainable production of cooling, clean water and domestic hot water in the United Arab Emirates [20]. Sonsaree et al. used CPC to drive a small-scale solar ORC power plant in Thailand [21]. Dai et al. analyzed a hybrid solar hot water and Bi_2Te_3-based thermoelectric generator unit using a heat pipe with mini-CPCs [22]. Brogren et al. discussed the optical efficiency of a water-cooled PV-thermal (PVT) system with low-concentration CPCs for high latitudes [23]. Tiwari et al. analyzed the influence of water and condensing cover temperatures on the yield and electrical power output of a PVT-CPC active solar distillation system [24]. Sharma et al. carried out energy, exergy, environmental impact, and economic analyses of solar CPC-powered thermal domestic SWH systems [25]. Arunkumar et al. analyzed the performance of CPC-assisted tubular/concentric solar stills with different augmentation systems [26].

The V-shaped and trapezoidal-shaped cavities are usually used as the secondary reflector of the STCs. Zheng et al. proposed a new multi-cavity receiver STC, and their study showed that compared with the traditional STC, the multi-cavity receiver STC can achieve more sunlight absorption, higher heat transfer rate, and better temperature distribution at the receiver outer surface [27]. Wang et al. analyzed the relationship between the concentration ratio and the gap efficiency of a V-shaped cavity CPC using the MCRT method [28]. Reddy and Satyanarayana developed a 3-D numerical model to evaluate the performance of the receiver with square, triangular, trapezoidal and circular shapes [29]. Wang et al. designed an inverted trapezoidal cavity receiver with an absorber of a bundle of tubes [30]. Venegas-Reyes et al. simulated the optical performance of a circular trough solar concentrator with a trapezoidal secondary reflector [31].

The trough concentrators will generate uneven energy flow distribution on the absorber's outer surfaces. That will lead to large thermal stress and damage of absorbers in solar thermal applications; and also cause hot spots, current mismatch and efficiency reduction in the PV systems. To solve this problem, Yang et al. proposed a surface-uniform-concentrator (SUC) and evaluated its optical performance in a solar photocatalytic hydrogen production system by using the MCRT method. They found that the solar energy conversion efficiency of the SUC is 8.57% higher than that of the CPC [32]. Wei et al. experi-

mentally used the SUC for solar photocatalytic hydrogen production, which validated the advantages of the SUC [33]. With respect to the thermal deformation due to the uneven solar flux on the STC receivers, Cao et al. carried out thermal performance and stress analyses of the cavity receiver in the PTCs [34]. Wang et al. developed a thermodynamic model to predict the thermal deformation of different cases for the preheating, boiling and superheating sections of a DSG-PTC loop [35]. Zhang et al. carried out optical sensitivity analysis of geometrical deformation on the PTC with the MCRT method [36].

There are few studies both compared the optical and thermal performances of different STC types. To give directions for scholars and engineers on choosing the STC type in different application fields, the frequently used STC types, viz. the PTC, the CPC, the SUC and the TTC, are compared in the present study. Their optical performances are first simulated using the MCRT method to obtain solar radiation distributions on the receivers. Their thermal performances, viz. the temperature distribution, the thermal deformation and equivalent stress, are then compared by applying the STCs to an SWH system.

2. Models and Methods

2.1. PTC

Figure 1 shows the schematic of a PTC model. According to Figure 1, P is the focal point of the parabola and ϕ is the circumference angle of the absorber tube. The reflector of the PTC is defined as [37]:

$$y^2 = 4fz \tag{1}$$

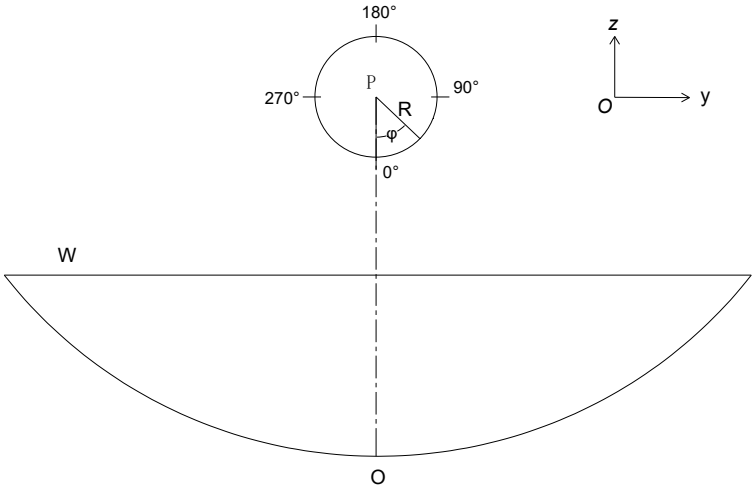

Figure 1. Schematic of a PTC model.

The PTC structure is determined by the focal length OP (viz. f in Equation (1)), the opening width W and the absorber tube radius R.

The concentration ratio C of the PTC is defined as the ratio between the solar collecting area A_a and the absorber tube area A_r:

$$C = \frac{A_a}{A_r} = \frac{W}{2\pi R} \tag{2}$$

2.2. CPC

The cross-section of a CPC is shown in Figure 2. According to Figure 2, the reflector of the CPC is symmetrical with the focal line, which is composed of two groups of evolvent-curves (BC and CD) and parabolic curves (AB and DE).

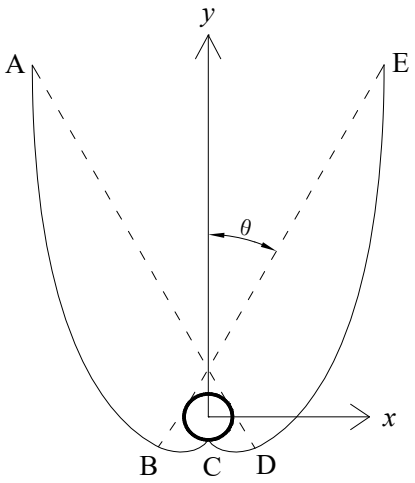

Figure 2. Schematic of a CPC model.

The curve *CD* is defined as [37]:

$$\begin{cases} x = R(\sin\varphi - \varphi\cos\varphi) \\ y = -R(\cos\varphi + \varphi\sin\varphi) \end{cases} \left(\theta \le \varphi \le \frac{\pi}{2} + \theta\right) \tag{3}$$

The curve *DE* is defined as [37]:

$$\begin{cases} x = R(\sin\varphi - \varphi'\cos\varphi) \\ y = -R(\cos\varphi + \varphi'\sin\varphi) \end{cases} \left(\frac{\pi}{2} + \theta \le \varphi \le \frac{3\pi}{2} - \theta\right) \tag{4}$$

where,

$$\varphi' = \frac{\frac{\pi}{2} + \theta + \varphi - \cos(\varphi - \theta)}{1 + \sin(\varphi - \theta)} \tag{5}$$

where θ is the acceptance half-angle of the CPC.

The concentration ratio *C* of the CPC is defined as:

$$C = \frac{1}{\sin\theta} \tag{6}$$

2.3. SUC

The cross-section of a SUC is shown in Figure 3. The SUC is composed of two symmetrical curves *AC* and *BD* and a line *CD*.

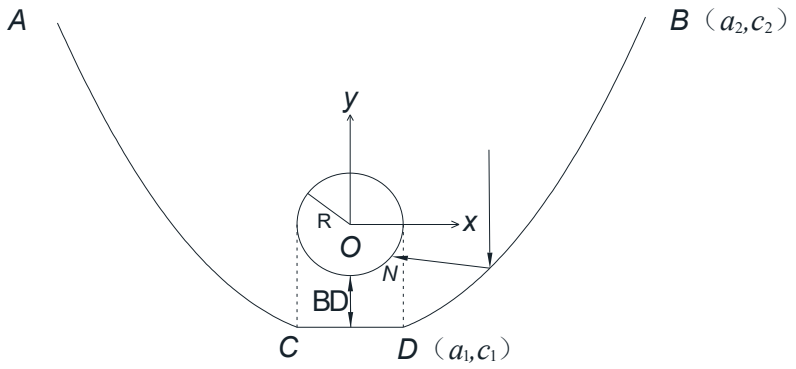

Figure 3. Schematic of a SUC model.

The curve *BD* is defined as [32]:

$$\frac{dy}{dx} = f(x,y) = \frac{x - x_b}{y_b - y + \sqrt{(x_b - x)^2 + (y_b - y)^2}} \tag{7}$$

where, (x_b, y_b) is the coordinate of *N*.

The concentration ratio *C* of the SUC is defined as:

$$C = \frac{a_2}{\pi R} \tag{8}$$

2.4. TTC

The cross-section of a TTC is shown in Figure 4. According to Figure 4, the reflector is an isosceles trapezoid. The main parameters of the TTC are the reflecting surface inclination angle δ, the centre height of the absorber tube H, the vertical height of the reflector h, the opening width of the concentrator W and the radius of the absorber tube R.

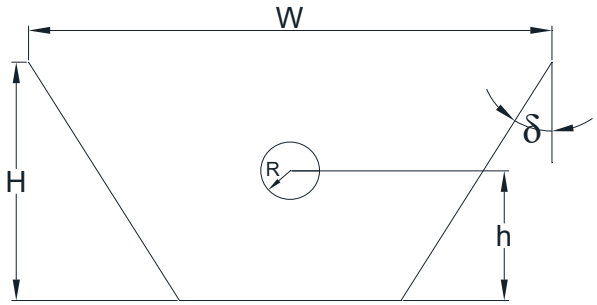

Figure 4. Schematic of a TTC model.

The concentration ratio C of the TTC is defined as:

$$C = \frac{W}{2\pi R} \tag{9}$$

To identify the surface radiation distribution uniformity on the absorber tube, the uniform index U is defined, which is [32]:

$$U = 1 - \frac{B_{\max} - B_{\min}}{B_{\max} + B_{\min}} \tag{10}$$

where $B_{\max}$ and $B_{\min}$ are the maximum and minimum solar radiation on the absorber.

2.5. Geometry of the STCs

The geometry parameters of the STCs are summarized in Table 1. According to Table 1, the PTC concentration ratio is much larger than the other three STCs'. The PTCs are recognized as high-concentration reflectors, mainly used for high-temperature solar thermal utilization, such as solar thermal power generation, auxiliary heat source, etc. The CPC, SUC and TTC are recognized as low-concentration reflectors, mainly used for domestic SWH, solar photocatalysis or PV power generation.

Table 1. Geometrical parameters of the concentrators.

STC Type	Parameter	Value	Concentration Ratio, C
PTC	Opening width, W	5 m	22.75
	Absorber tube radius, R	0.035 m	
	Tube length, L	1 m	
CPC	Acceptance half-angle, θ	30°	2
	Absorber tube radius, R	0.035 m	
	Tube length, L	1 m	
SUC	Absorber tube radius, R	0.02 m	4
	Bottom distance, BD	0.04 m	
	Tube length, L	1 m	

Table 1. *Cont.*

STC Type	Parameter	Value	Concentration Ratio, *C*
TTC	Opening width, *W*	0.18 m	1.21
	Absorber tube radius, *R*	0.02 m	
	Height, *H*	0.05 m	
	Absorber tube central height, h	0.03 m	
	Reflector tilted angle, θ	36°	
	Tube length, *L*	1 m	

2.6. Simulation Methods

The simulation methods in this research are shown in Figure 5. The solar ray tracing results of four STCs are first simulated using the MCRT method in TracePro software. The simulation process and input parameters are shown in Figure 5. The obtained solar radiation distribution on the absorber tube outer surface is then introduced into ANSYS Fluent to simulate the thermal performance of the STCs, viz. the absorber wall temperature distribution and the fluid temperature field. The thermal simulation results are then introduced as the thermal condition into ANSYS Workbench to simulate the static structure deformation and stress of the STCs' absorber tubes.

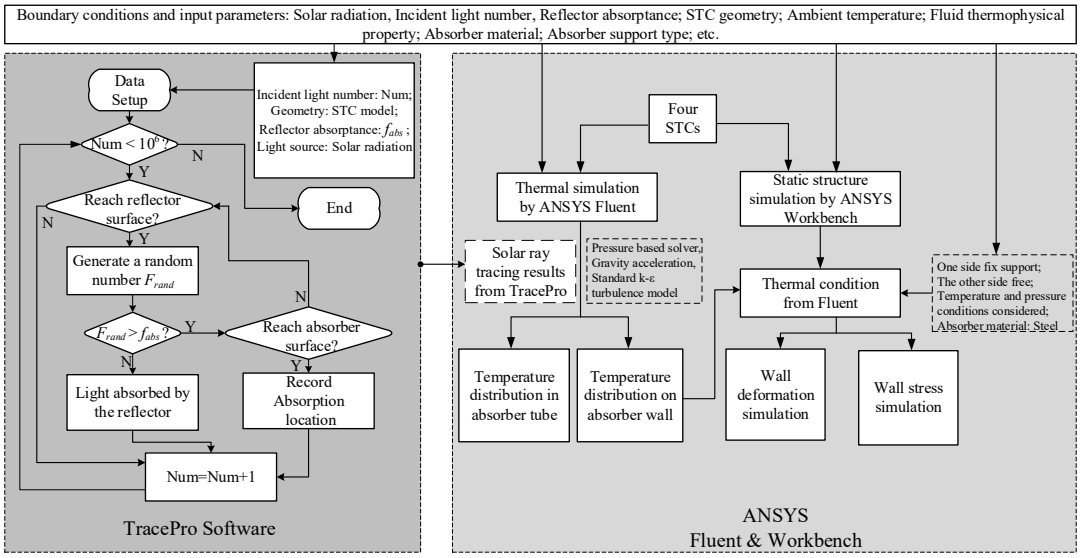

Figure 5. Simulation methods in this study.

3. Results and Discussion

3.1. Model Validation

The MCRT method is used to simulate the optical performances of the STCs. The correctness of the developed models and the MCRT method in this paper is verified by comparing the simulated distribution of heat flux in the circumferential direction of the absorber outer surface with reported data in the literature. The PTC absorber heat flux distribution from Ref. [38] and the simulated results in the present study are compared in Figure 6. It is found in Figure 6 that good agreement is found between the simulated results and the results in Ref. [38]. So, the mathematical model built in this study and the MRCT method is ready to simulate the optical performances of the four STCs.

During the MCRT simulation, several assumptions are applied: (1) Parallel light is emitted perpendicular toward the STC opening surface with a uniform wavelength; (2) The incident solar radiation intensity is 1000 W/m^2; (3) The tracking error of the STC is ignored, and the solar incidence angle is 0°; (4) The number of incident light is 1,000,000;

(5) Only direct radiation is considered in the simulation, and (6) The reflectivity of STC reflector is assumed to be 1.

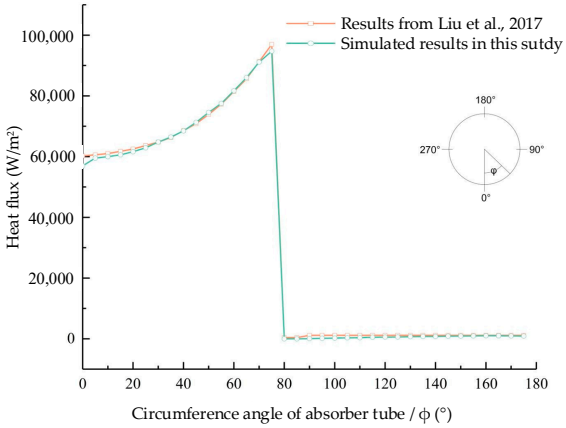

Figure 6. Comparison of PTC radiation distribution on the absorber outer surface between the simulated results in this study and Liu, et al., 2017 (Ref. [38]).

3.2. Ray Tracing Results

3.2.1. PTC Results

The solar ray tracing results, the average solar radiation at the cross-section, and the radiation distribution of the absorber upper and lower surfaces of the PTC are shown in Figure 7a–d respectively. According to Figure 7a,b, the average solar radiation at the cross-section of the PTC absorber is symmetrically distributed at 180°, and there are two peaks located at 55° and 310° respectively. The heat flux of the PTC absorber is uneven along the circumferential direction, with a maximum value of 66,535 W/m^2 at 55° and 310°, and the minimum value of is 0 W/m^2 in 70°–90° and 270°–290°. Statistical results show that the average heat flux on the PTC absorber tube is 22,591.33 W/m^2. The circumferential radiation distribution of the absorber tube can be divided into four areas, viz. the shielding area, the increasing area, the attenuation area and the direct incidence area. According to an enlarged view of the absorber tube in Figure 7a, the incident light is blocked by the absorber tube at 0°, leading to a sudden drop of heat flux, which is called the shielding area. Due to the increase of reflected light, the heat flux density increases continuously at 0°–55°, which is called the increasing area. The heat flux decreases rapidly due to the continuous reduction of reflected light near 70°, which is called the attenuation area. Only direct radiation can be absorbed by the absorber at 90°–180°, whose heat flux is the initial solar radiation of 1000 W/m^2. This range is called the direct incidence area. According to Figure 7c,d, the radiation distribution along the radial direction of the absorber is uniform.

3.2.2. CPC Results

The solar ray tracing results, the average circumferential solar radiation at the cross-section, and the radiation distribution of the CPC absorber upper and lower surfaces along the radial direction are shown in Figure 8a–d respectively. According to Figure 8a,b, the average solar radiation at the cross-section of the CPC absorber is symmetrically distributed at 180°, and there are two peaks located at 65°, 300° and one secondary peak at 0° respectively. At 65° and 300°, most of the incident light is focused after one reflection, whereas at 0° (also 360°), the incident light reaches the absorber after multiple reflections resulting in greater reflection loss at 0°, which leads to the different peak values. The heat flux of the CPC absorber is fluctuating wildly in the circumferential direction. The maximum solar radiation of 10,597 W/m^2 locates at 65° and 300°. The secondary peak value of 4671.6 W/m^2 locates at 0°. The minimum value is 0 W/m^2 at 85° and 275°, where no direct and reflected radiation reaches. Statistical results show that the average heat flux

on the CPC absorber tube is 1998.48 W/m^2. It can be seen from Figure 8c,d that the radial radiation distribution on the absorber along the radial direction is uniform.

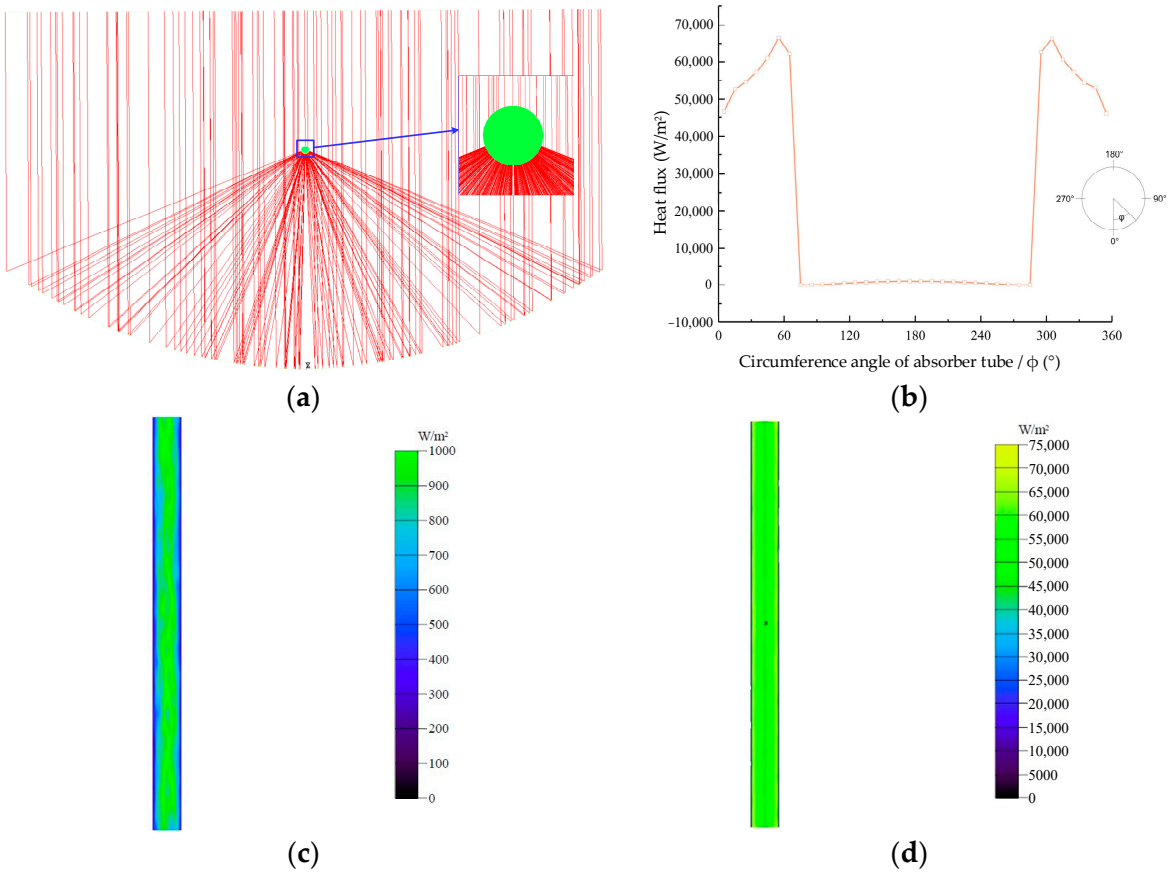

Figure 7. (**a**) PTC solar ray tracing results (including an enlarged view of the absorber tube), (**b**) average circumferential solar radiation at the cross-section, (**c**) Upper surface solar radiation distribution along the radial direction, (**d**) lower surface solar radiation distribution along the radial direction.

3.2.3. SUC Results

The solar ray tracing results, the average solar radiation at the cross-section, and the radiation distribution of the SUC absorber upper and lower surfaces along the radial direction are shown in Figure 9a–d respectively. It can be seen from the figures that more uniform solar radiation distribution is found on the SUC receivers than those of the PTC and CPC receivers. The circumferential radiation distribution is also symmetrical at 180°, and it is fluctuant in a small range between 3577 W/m^2 and 4610 W/m^2, with the average being 3941.54 W/m^2. Moreover, it is found that the heat flux on the upper surface of the absorption tube is greater than the initial incident radiation of 1000 W/m^2, which indicates that the SUC's reflector can reflect incoming light to the range of 0° to 360°. According to previous analyses, the PTC and CPC mainly concentrate the incident light on both sides of the lower surface of the absorber tube and they mainly absorb direct solar radiation on the upper surface. So, their heat flux on the lower surface is greater than that on the upper surface. However, the heat flux on the upper surface of the SUC heat absorption tube is greater than that on the lower surface within the range of 90° to 270°. This is because the lower surface of the absorber only absorbs reflected light, whereas both direct and reflected light are received on the upper surface of the absorber. The superposition of the two kinds of radiation makes the upper surface heat flux larger than the lower surface heat flux. The difference between the maximum and the minimum heat flux of the SUC is 1033 W/m^2, which denotes the high uniformity of the SUC.

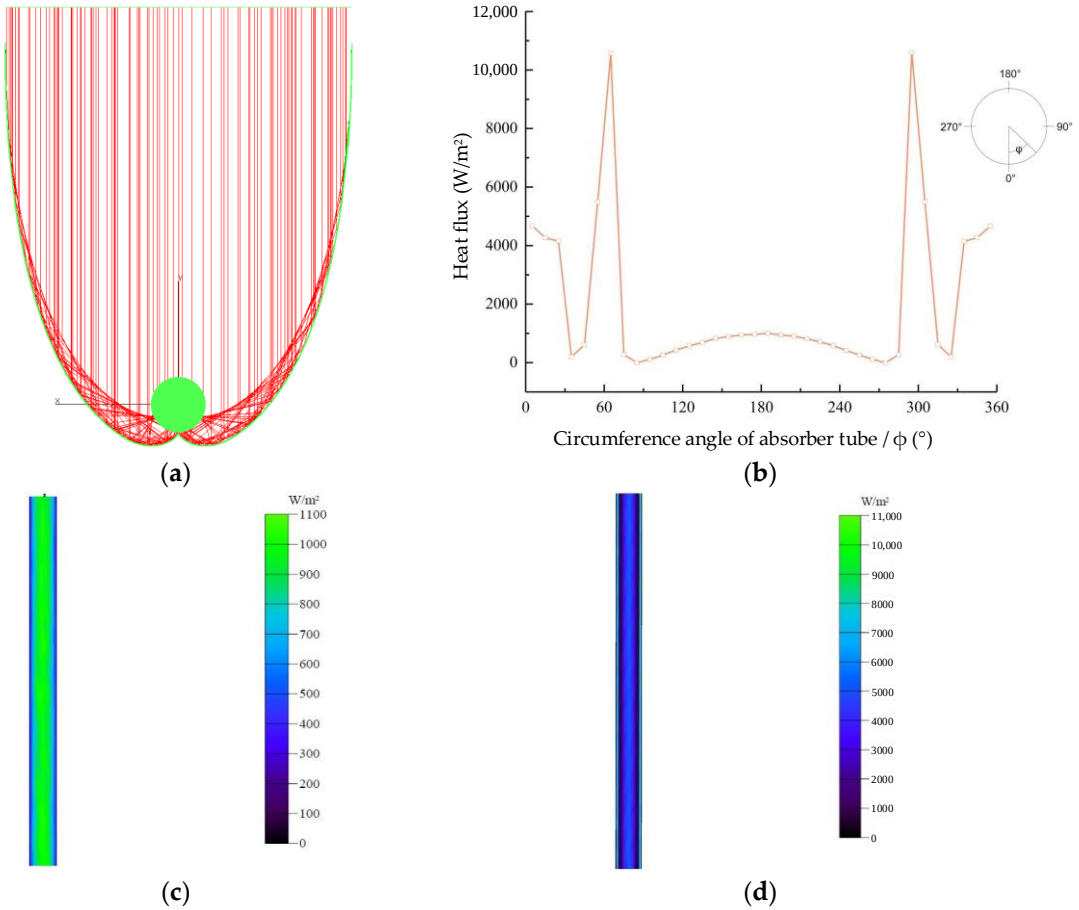

Figure 8. (**a**) CPC solar ray tracing results, (**b**) average circumferential solar radiation at the cross-section, (**c**) upper surface solar radiation distribution along the radial direction, (**d**) lower surface solar radiation distribution along the radial direction.

3.2.4. TTC Results

The solar ray tracing results, the average circumferential solar radiation at the cross-section, and the radiation distribution of the TTC absorber upper and lower surfaces along the radial direction are shown in Figure 10a–d respectively. Compared with the PTC and CPC, the radial and the circumferential radiation distributions of the TTC are more uniform, because of their symmetrical structure. In addition, there is a dark area at the bottom of the absorber in the range of −30°–+30°, where incident and reflected light are shielded by the absorber. There are two peaks of 1171.9 W/m^2 at 125° and 235° respectively. There are also two secondary peaks of 991.31 W/m^2 at 75° and 285°. The reason for their difference is that the absorber only absorbs the reflected radiation at the secondary peak, while there is a superposition of direct and reflected radiation at the peak. Only direct incident light reaches the absorber in the range of 160°–180°. The average heat flux on the TTC absorber is only 845.91 W/m^2.

3.3. Absorber Tube Radiation Distribution Comparison

To compare the optical performance of the four STCs, four evaluation parameters, namely, the central angle of reflected light, the non-light central angle, the light reception ratio and the uniformity, are proposed. The central angle of reflected light refers to the maximum range of reflected light on the surface of the absorber. The non-light central angle refers to the region where the absorber does not receive any light. The light reception ratio refers to the proportion of the amount of light received on the surface of the absorber

to the amount of incident light. The uniformity is calculated according to Equation (10). Comparison results of the optical performance of four STCs are shown in Table 2.

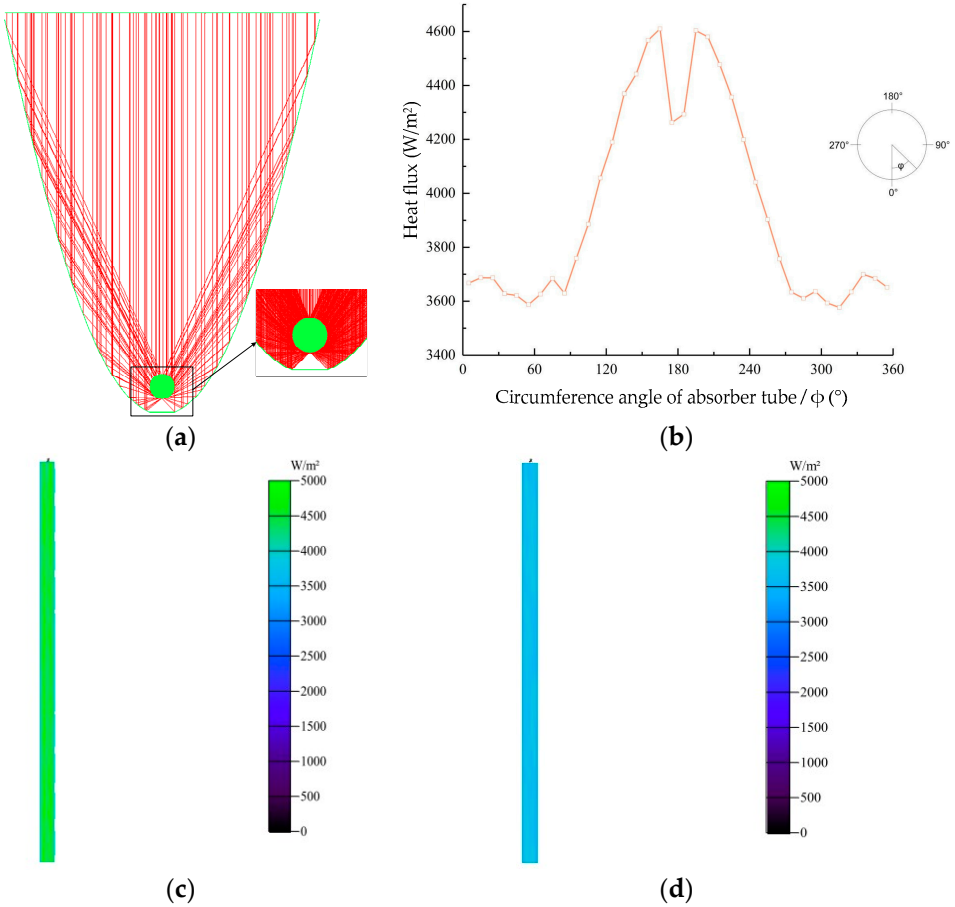

Figure 9. (**a**) SUC solar ray tracing results (including enlarged view near the absorber tube), (**b**) average circumferential solar radiation at the cross-section, (**c**) upper surface solar radiation distribution along the radial direction, (**d**) lower surface solar radiation distribution along the radial direction.

Table 2. Comparison of optical results of four STCs.

STC Type	Central Angle of Reflected Light (°)	None-Light Central Angle (°)	Light Reception Ratio (-)	Uniformity (-)
PTC	140	40	100%	0.32%
CPC	160	20	100%	2.12%
SUC	360	0	100%	87.38%
TTC	260	60	70%	80.50%

According to Figures 7–10 and Table 2, it is found that the PTC has the worst uniformity among the four STCs, which is only 0.32%. Its reflected light distributes in the region of 140°, where the heat flux on the absorber tube is greater than the initial solar radiation of 1000 W/m^2. In addition, there is a non-light incident region of 40° on the PTC absorber. The reflected light distribution range of the CPC is 160°. But the actual angle range where the heat flux is greater than 1000 W/m^2 is 100°, and there is a non-light incident region of 20° on the CPC absorber. Compared with the CPC and the PTC, the light distribution on the TTC absorber tube is more uniform. but the TTC's light reception ratio is poorer, whose no-light area reaches 1/6 of the whole surface. Compared with the other three STCs, the SUC holds the highest uniformity of 87.38%, and its reflected light can reach every location of the absorber.

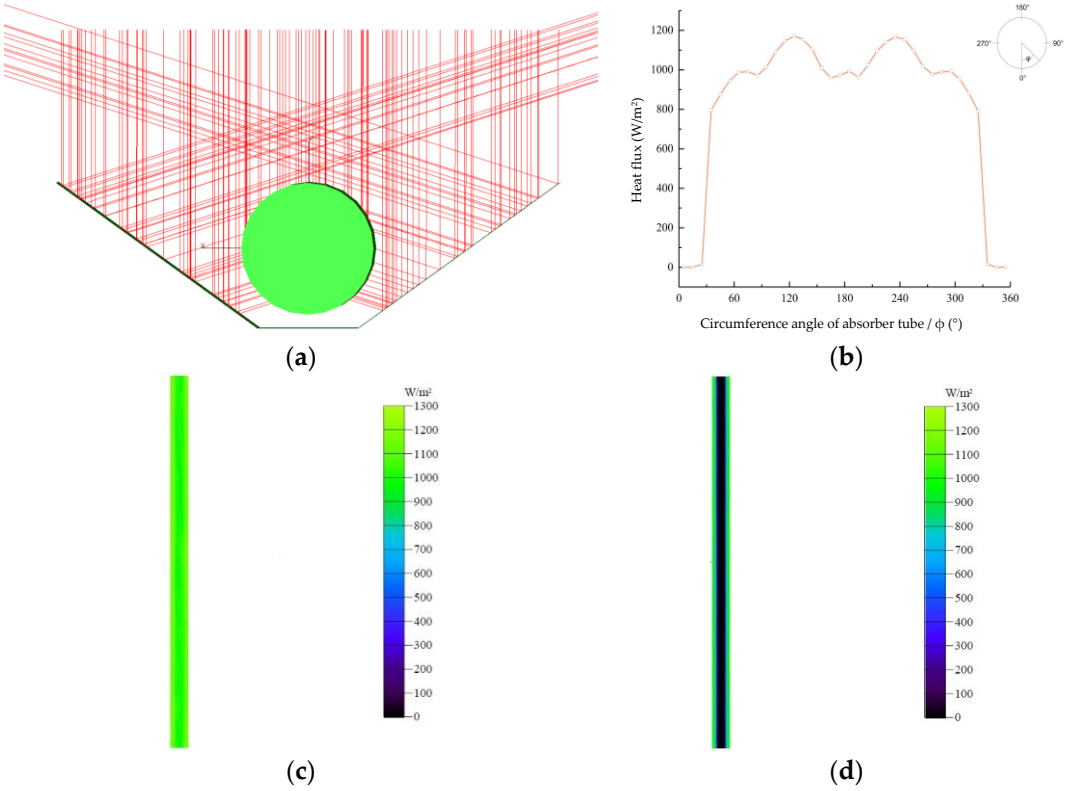

Figure 10. (**a**) TTC solar ray tracing results, (**b**) average circumferential solar radiation at the cross-section, (**c**) Upper surface solar radiation distribution along the radial direction, (**d**) lower surface solar radiation distribution along the radial direction.

3.4. Performance Evaluation in an SWH System

To compare the thermal performance of the PTC, CPC, SUC and TTC, the STCs are introduced into an SWH system. The cold water comes into the SWH system from one side of the absorber, and goes out of the SWH system on the other side, as shown in Figure 11. Five typical cross-sections are used to compare their thermal performances. The parameters used in the simulation are summarized in Table 3.

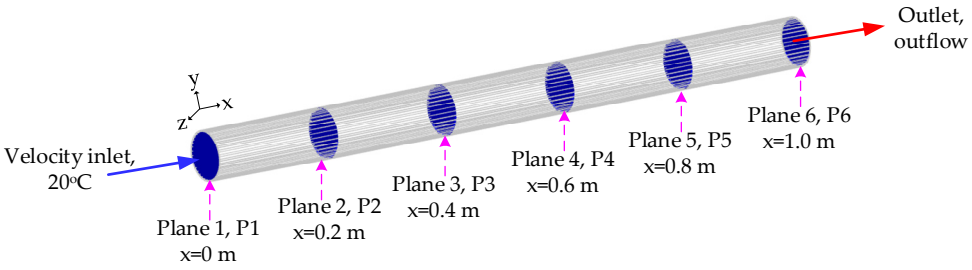

Figure 11. Schematic of the STC receiver in the SWH system.

3.4.1. Comparison of Top and Bottom Wall Temperature Distributions

The top and bottom wall temperatures of four STCs in the SWH systems are shown in Figure 12a–d. It can be seen from the figures that the PTC wall temperatures are much higher than the other three STCs' even though the PTC inlet water velocity is twice the other three STCs', due to the much higher concentration ratio of the PTC. Because of the solar radiation distribution as shown in Figures 7 and 8, the top wall temperatures of the PTC and CPC are much smaller than those at the bottom. But, according to Figure 12d, the top wall temperature of the TTC is larger than that at the bottom, which is also a result of the solar radiation distribution as shown in Figure 10. The temperature uniformity

at the cross-section of the SUC is the best among the four STCs. And the highest wall temperatures match well with the STCs' solar concentration ratio in Table 1.

Table 3. Parameters in thermal performance system of the four STCs.

STC Type	Inlet			Outlet	Outer Wall
	Boundary Condition	Velocity	Temperature	Boundary Condition	Heat Flux
PTC	Velocity inlet	0.02 m/s [1]	20 °C	Outflow	Solar ray-tracing results as shown in Figure 7
CPC	Velocity inlet	0.01 m/s	20 °C	Outflow	Solar ray-tracing results as shown in Figure 8
SUC	Velocity inlet	0.01 m/s	20 °C	Outflow	Solar ray-tracing results as shown in Figure 9
TTC	Velocity inlet	0.01 m/s	20 °C	Outflow	Solar ray-tracing results as shown in Figure 10

Note: [1] As the PTC concentration ratio is much higher than the other three STCs, its inlet velocity is larger than the others, otherwise the water temperature may be over 100 °C.

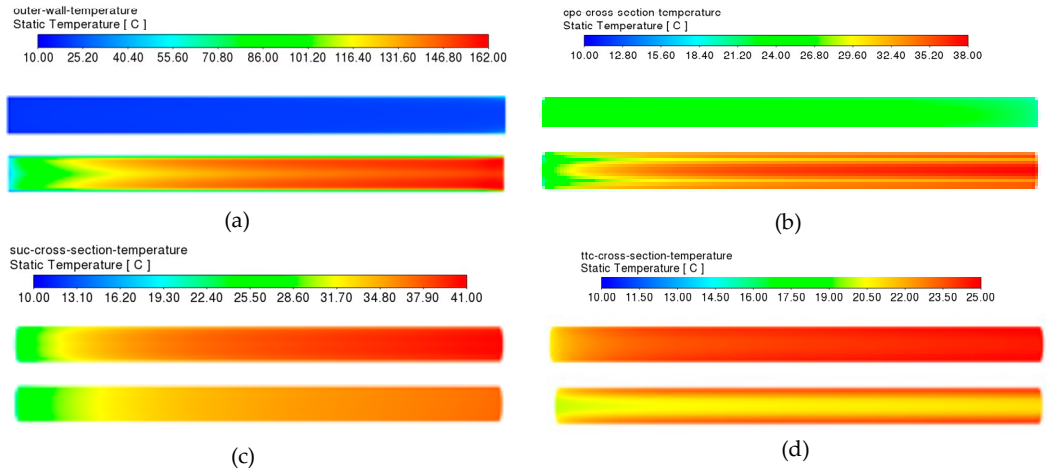

Figure 12. The top wall and bottom wall temperatures of (**a**) the PTC, (**b**) the CPC, (**c**) the SUC and (**d**) the TTC in the SWH systems, where the above figure and below figure refer to the top wall and bottom wall respectively, and the left side and right side are the water inlet and outlet respectively.

3.4.2. Comparison of Cross-Section Temperature Distribution

The cross-section temperatures of the four STCs in the SWH systems are shown in Figure 13. It can be seen from Figure 13Aa–f that, due to the high solar flux at the bottom of the PTC, the wall and water temperatures at the bottom are much higher than those in the other locations. And according to Figure 13Ag, the hot water temperature area linearly increases and finally takes nearly 1/5 of the cross-section at the outlet. Figure 13Ah shows the water temperature rises gradually along the horizontal central cross-section. The PTC holds the highest water temperature rise among the four STCs.

Three peaks can be found at the cross-sections of the CPC according to Figure 13Ba–f, which are at the bottom and 60° off the bottom. That fits well with the solar flux distribution in Figure 8b. The water temperatures near these areas are slightly higher than those in the other areas. The vertical cross-section temperature in Figure 13Bg shows the water temperature near the bottom is slightly higher than that in the other area, and the hot area takes nearly 1/10 of the cross-section at the water outlet.

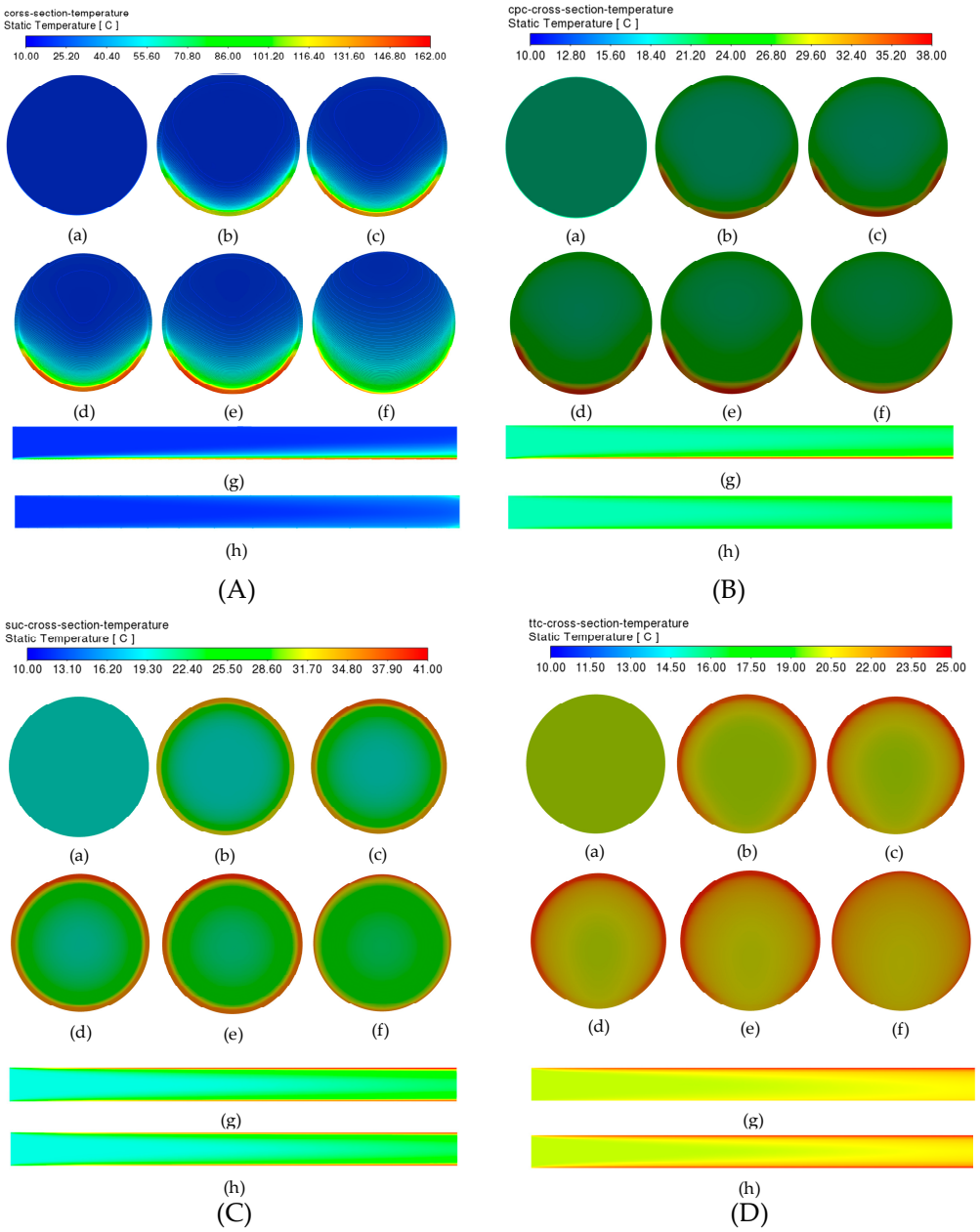

Figure 13. The cross-section temperature distributions of (**A**) the PTC, (**B**) the CPC, (**C**) the SUC and (**D**) the TTC in the SWH systems at (**a**) P1, (**b**) P2, (**c**) P3, (**d**) P4, (**e**) P5, (**f**) P6, (**g**) central cross-section along the absorber in x-y (vertical) plane, and (**h**) central cross-section along the absorber in x-z (horizontal) plane.

According to Figure 13Ca–f, the water temperature near the absorber is higher than that in the centre due to the uniform solar irradiation. As shown in Figure 13Cg,h, the water temperature along the horizontal cross-section is similar to that along the vertical cross-section, which validates the best uniformity of the SUC.

Unlike the other three STCs, according to Figure 13D, the water temperature near the top wall of the TTC is higher than that near the bottom, which is a result of the solar flux distribution as shown in Figure 10. The water temperature rise of the TTC is the smallest among the four STCs.

3.4.3. Thermal Deformation Comparison

The steel absorber thermal deformation and equivalent stress of the four STCs in the SWH systems are shown in Figure 14A–D respectively. The STCs' thermal deformations

are positively correlated to their wall temperatures in Figure 12, with the highest thermal deformation of 9.9322 mm in PTC and the smallest thermal deformation of 0.2007 mm in TTC. And the receivers deform towards the direction of low-temperature areas. Due to the uniform temperature distribution, the radial deformation of the SUC is much larger than those of the other three STCs. It can also be found from Figure 14A–Db that, the smallest equivalent stress of 7.6525 MPa is found in the SUC, which is beneficial to the long-term operation of the SWH system. The highest equivalent stress of 165.52 MPa is found in PTC, due to the highest solar flux and wall temperature.

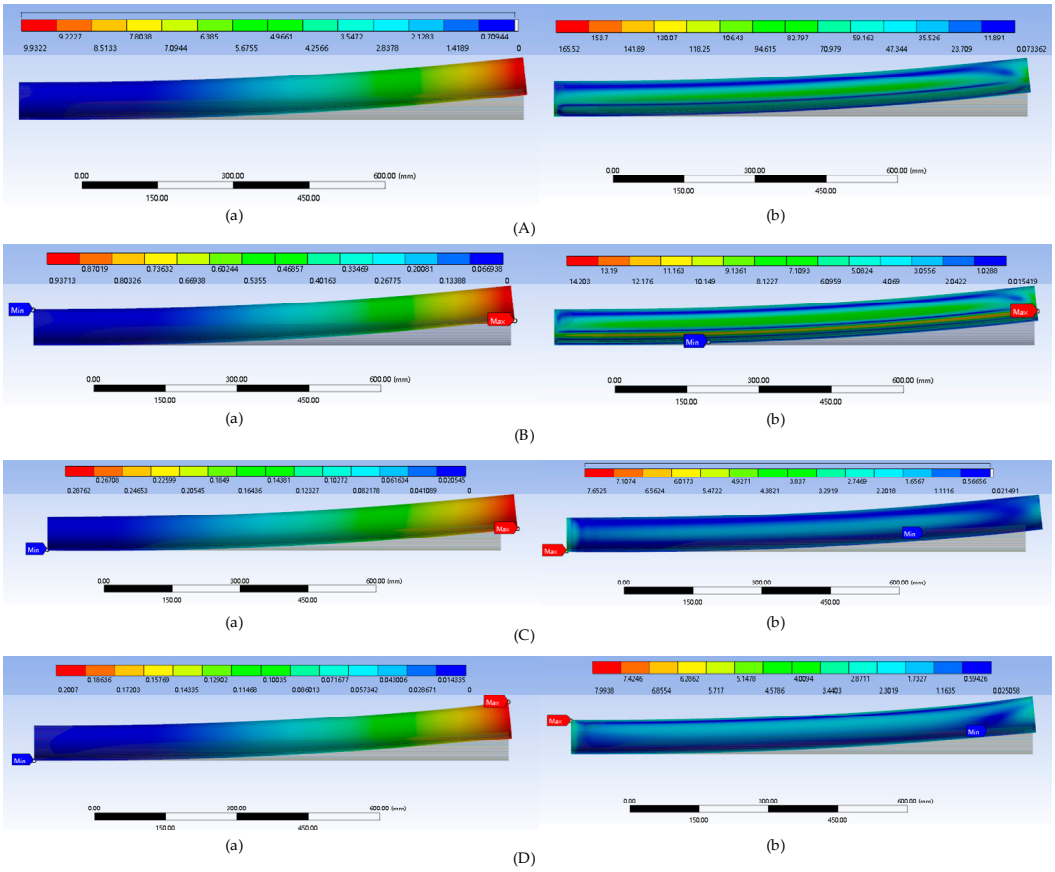

Figure 14. The steel absorber thermal deformation and equivalent stress of (**A**) the PTC, (**B**) the CPC, (**C**) the SUC and (**D**) the TTC in the SWH systems where (**a**) is the thermal deformation (Unit: mm), (**b**) is the equivalent stress (Unit: MPa). Note that the shadow in the figures are the location of the original tube receivers.

3.5. STC Application

The STCs can be combined with different receivers, including circular tubes [1–21,25,26], flat plates [22–24], cavity receivers [27–31], etc. The STCs are used to increase the solar radiation intensity on absorbers for SWH [3,7,26], DSG [11,35], desalination [6,13,14] and solar thermal/PV power generation [5,22,24,25] purposes. After optical, thermal and deformation comparisons of four STCs, it can be found that the PTC has the highest concentration ratio and heating performance. The PTC can be combined with all absorber types for heating purposes as the incoming heat flux is high and can reach the full area of the absorber. The PTC is thus suggested to be used in high-temperature thermal, DSG, and concentrated PV (CPV) purposes. The CPC, especially the truncated CPC has a low concentration ratio but benefits from its simple structure and low cost. The CPC can be combined with all the absorber types as sunlight can reach all areas of its receiver. It can be used for low-temperature solar thermal applications, such as the SWH and solar desalination. The CPC can also be used for solar photocatalysis purposes, as

the truncated reflector can also reflect the diffused solar radiation, in which the ultraviolet radiation is high. Cao et al. have designed and constructed a pilot direct solar photocatalyst water-splitting system for hydrogen generation using the CPC modules [39,40]. The SUC can hardly be combined with the flat plate receivers due to its special-designed geometry. The SUC have the highest uniformity, thus it can be used for solar PV purposes. The SUC is also suggested to be used in solar photocatalysis purposes, where photocatalysts are evenly dispersed in the solution. Too high local solar radiation or uneven solar radiation distribution on the absorber would lead to agglomeration and disability of the photocatalysts [32,33]. The TTC holds high uniformity but low light reception and concentration ratio. Considering its simple structure and low cost, it is usually combined with flat plate receivers and used for solar PV purposes. The detailed STC characteristics and their suggested application fields are summarized in Table 4.

Table 4. STC application suggestions.

STC Type	Light Reception	Uniformity	Concentration Ratio	Absorber Types	Application Field
PTC	Full area	Low	High	Circular tubes, flat plates, cavity receivers	High-temperature solar thermal, DSG, CPV
CPC	Full area	Low	Low	Circular tubes, flat plates, cavity receivers	Solar thermal, solar photocatalysis, solar desalination
SUC	Full area	High	Low	Circular tubes, cavity receivers	Solar thermal, solar photocatalysis, solar PV
TTC	Part area	High	Low	Flat plates, cavity receivers	Solar thermal, solar PV

4. Conclusions

In the present study, optical and thermal performances of four STC types, viz. the PTC, the CPC, the SUC and the TTC, are compared using numerical simulation methods. The main conclusions of this study are summarized as follows:

(1) As a concentrator with a high concentration ratio, PTC has the highest solar flux with two peaks at 55° and 305° on the receiver cross-section. The CPC can generate the highest heat flux among the three low concentrators (viz. the CPC, the SUC and the TTC). There are two peaks at 65° and 300° and one secondary peak at 0° on the cross-section of the CPC. There is a dark area at the bottom of the TTC at the angle of −30°–+30° due to the absorber shielding. More uniform solar radiation distribution is found on the SUC receivers than that on the other three STCs.

(2) The PTC has the worst uniformity of 0.32% among the four STCs. Compared with the CPC and the PTC, the light distribution on the TTC absorber tube is more uniform. But the TTC's light reception ratio is poorer, whose no-light area reaches 1/6 of the whole surface. The SUC holds the highest uniformity of 87.38%, and its reflected light can reach every location of the absorber.

(3) The PTC wall temperatures are much higher than the other three STCs' even though the PTC inlet water velocity is twice the other three STCs'. The top wall temperatures of the PTC and CPC are much smaller than those at the bottom. The top wall temperature of the TTC is larger than that at the bottom. The temperature uniformity at the cross-section of the SUC is the best among the four STCs. The water temperatures inside the STCs are directly in response to their wall temperature, with the highest temperature rise in the PTC and the smallest in the TTC.

(4) The STCs' thermal deformations are positively correlated to their wall temperatures. And the receivers deform towards the direction of low-temperature areas. The radial deformation of the SUC is much larger than those of the other three STCs. The highest

equivalent stress is found in PTC. The smallest equivalent stress is found in the SUC, which is beneficial to the long-term operation of the SWH system.

Author Contributions: Conceptualization, F.C. and J.P.; methodology, X.G. and M.W.; validation, M.W. and F.C.; formal analysis, F.C. and M.W.; writing—original draft preparation, F.C.; writing—review and editing, Y.S.; funding acquisition, F.C. All authors have read and agreed to the published version of the manuscript.

Funding: This research was funded by the Natural Science Foundation of Jiangsu Province [No.: BK20201161] and the Natural Science Foundation of China [No.: 51506043].

Data Availability Statement: The data presented in this study are available in Figures 7–10 and 12–14 of this paper.

Conflicts of Interest: The authors declare no conflict of interest.

Nomenclature

A_a	Solar collecting area [m^2]
A_r	Absorber tube area [m^2]
STC	Solar trough concentrator
BD	Bottom distance [m]
B_{max}	Maximum solar radiation on the absorber [W/m^2]
B_{min}	Minimum solar radiation on the absorber [W/m^2]
C	Concentration ratio
CPC	Compound parabolic concentrator
DSG	Direct steam generation
f	Focal length [m]
f_{abs}	Absorptance of the wall
F_{rand}	Random number between 0 and 1
H	Center height of the absorber tube [m]
h	Vertical height of the reflector [m]
L	Tube length [m]
MED-VC	Multi-Effect Distillation-Vapor Compression
MCRT	Monte Carlo Ray Tracing
NUM	Incident light number
ORC	Organic Rankine cycle
P	Focal point of the parabola
PTC	Parabolic trough concentrator
PVT	PV-thermal
R	Absorber tube radius [m]
SWH	Solar water heating
SUC	Surface uniform concentrator
TTC	Trapezoid trough concentrator
U	Uniform index
W	Opening width [m]
Greek symbols	
ϕ	Circumference angle of absorber tube [°]
θ	Acceptance half-angle of the CPC [°]
δ	Reflecting surface inclination angle [°]

References

1. Padilla, R.V.; Demirkaya, G.; Goswami, D.Y.; Stefanakos, E.; Rahman, M.M. Heat transfer analysis of parabolic trough solar receiver. *Appl. Energy* **2011**, *88*, 5097–5110. [CrossRef]
2. Wang, Q.L.; Yang, H.L.; Hu, M.K.; Cao, J.Y.; Pei, G.; Yang, H.X. Optimization strategies and verifications of negative thermal-flux region occurring in parabolic trough solar receiver. *J. Clean Prod.* **2021**, *278*, 123407. [CrossRef]
3. Avargani, V.M.; Divband, M. Performance evaluation of a solar water heating system with glass-covered parabolic trough concentrators under different system tracking modes. *J. Therm. Anal. Calorim.* **2022**, *147*, 4873–4888. [CrossRef]
4. Bellos, E.; Tzivanidis, C.; Antonopoulos, K.A.; Gkinis, G. Thermal enhancement of solar parabolic trough collectors by using nanofluids and converging-diverging absorber tube. *Renew. Energy* **2016**, *94*, 213–222. [CrossRef]

5. Freeman, J.; Hellgardt, K.; Markides, C.N. An assessment of solar-powered organic Rankine cycle systems for combined heating and power in UK domestic applications. *Appl. Energy* **2015**, *138*, 605–620. [CrossRef]
6. Nafey, A.S.; Sharaf, M.A. Combined solar organic Rankine cycle with reverse osmosis desalination process: Energy, exergy, and cost evaluations. *Renew. Energy* **2010**, *35*, 2571–2580. [CrossRef]
7. Zou, B.; Dong, J.K.; Yao, Y.; Jiang, Y.Q. An experimental investigation on a small-sized parabolic trough solar collector for water heating in cold areas. *Appl. Energy* **2016**, *163*, 396–407. [CrossRef]
8. Calise, F. High temperature solar heating and cooling systems for different Mediterranean climates: Dynamic simulation and economic assessment. *Appl. Therm. Eng.* **2012**, *32*, 108–124. [CrossRef]
9. Coccia, G.; Di Nicola, G.; Sotte, M. Design, manufacture, and test of a prototype for a parabolic trough collector for industrial process heat. *Renew. Energy* **2015**, *74*, 727–736. [CrossRef]
10. El Fadar, A.; Mimet, A.; Perez-Garcia, M. Study of an adsorption refrigeration system powered by parabolic trough collector and coupled with a heat pipe. *Renew. Energy* **2009**, *34*, 2271–2279. [CrossRef]
11. Sanda, A.; Moya, S.L.; Valenzuela, L. Modelling and simulation tools for direct steam generation in parabolic-trough solar collectors: A review. *Renew. Sustain. Energy Rev.* **2019**, *113*, 109226. [CrossRef]
12. Temiz, M.; Dincer, I. Concentrated solar driven thermochemical hydrogen production plant with thermal energy storage and geothermal systems. *Energy* **2021**, *219*, 119554. [CrossRef]
13. Sharaf, M.A.; Nafey, A.S.; Garcia-Rodriguez, L. Exergy and thermo-economic analyses of a combined solar organic cycle with multi effect distillation (MED) desalination process. *Desalination* **2011**, *272*, 135–147. [CrossRef]
14. Kabeel, A.E.; Elkelawy, M.; Alm, H.; Alghrubah, E.D.A. Investigation of exergy and yield of a passive solar water desalination system with a parabolic concentrator incorporated with latent heat storage medium. *Energy Convers. Manag.* **2017**, *145*, 10–19. [CrossRef]
15. Su, Z.; Gu, S.; Vafai, K. Modeling and simulation of ray tracing for compound parabolic thermal solar collector. *Int. Commun. Heat Mass.* **2017**, *87*, 169–174. [CrossRef]
16. Abdullahi, B.; AL-Dadah, R.K.; Mahmoud, S.; Hood, R. Optical and thermal performance of double receiver compound parabolic concentrator. *Appl. Energy* **2015**, *159*, 1–10. [CrossRef]
17. Ustaoglu, A.; Alptekin, M.; Okajima, J.; Maruyama, S. Evaluation of uniformity of solar illumination on the receiver of compound parabolic concentrator (CPC). *Sol. Energy* **2016**, *132*, 150–164. [CrossRef]
18. Waghmare, S.A.; Gulhane, N.P. Optical evaluation of compound parabolic collector with low acceptance angle. *Optik* **2017**, *149*, 359–371. [CrossRef]
19. Xu, R.J.; Zhang, X.H.; Wang, R.X.; Xu, S.H.; Wang, H.S. Experimental investigation of a solar collector integrated with a pulsating heat pipe and a compound parabolic concentrator. *Energy Convers. Manag.* **2017**, *148*, 68–77. [CrossRef]
20. Mohan, G.; Kumar, U.; Pokhrel, M.K.; Martin, A. A novel solar thermal polygeneration system for sustainable production of cooling, clean water and domestic hot water in United Arab Emirates: Dynamic simulation and economic evaluation. *Appl. Energy* **2016**, *167*, 173–188. [CrossRef]
21. Sonsaree, S.; Asaoka, T.; Jiajitsawat, S.; Aguirre, H.; Tanaka, K. A small-scale solar Organic Rankine Cycle power plant in Thailand: Three types of non-concentrating solar collectors. *Sol. Energy* **2018**, *162*, 541–560. [CrossRef]
22. Dai, Y.J.; Hu, H.M.; Ge, T.S.; Wang, R.Z.; Kjellsen, P. Investigation on a mini-CPC hybrid solar thermoelectric generator unit. *Renew. Energy* **2016**, *92*, 83–94. [CrossRef]
23. Brogren, M.; Nostell, P.; Karlsson, B. Optical efficiency of a PV-thermal hybrid CPC module for high latitudes. *Sol. Energy* **2000**, *69*, 173–185. [CrossRef]
24. Tiwari, G.N.; Mishra, A.K.; Meraj, M.; Ahmad, A.; Khan, M.E. Effect of shape of condensing cover on energy and exergy analysis of a PVT-CPC active solar distillation system. *Sol. Energy* **2020**, *205*, 113–125. [CrossRef]
25. Sharma, D.K.; Sharma, D.; Ali, A.H.H. Energy, exergy, environmental impact, and economic analyses of evacuated tube compound parabolic concentrator-powered solar thermal domestic water heating system. *Environ. Sci. Pollut. Res.* **2022**, *29*, 82390–82410. [CrossRef]
26. Arunkumar, T.; Velraj, R.; Denkenberger, D.C.; Sathyamurthy, R.; Kumar, K.V.; Ahsan, A. Productivity enhancements of compound parabolic concentrator tubular solar stills. *Renew. Energy* **2016**, *88*, 391–400. [CrossRef]
27. Zheng, H.F.; Tao, T.; Dai, J.; Kang, H.F. Light tracing analysis of a new kind of trough solar concentrator. *Energy Convers. Manag.* **2010**, *52*, 2373–2377. [CrossRef]
28. Wang, J.; Yu, L.; Jiang, C.; Yang, S.; Liu, T.T. Optical analysis of solar collector with new V-shaped CPC. *Sol. Energy* **2016**, *135*, 780–785. [CrossRef]
29. Reddy, K.S.; Satyanarayana, G.V. Numerical study of porous finned receiver for solar parabolic trough concentrator. *Eng. Appl. Comp. Fluid* **2008**, *2*, 172–184. [CrossRef]
30. Wang, Z.; Tian, R.; Qi, J.; Li, P.; Wei, Q. Structural Design and Optical Performance of Inverted Trapezoidal Cavity Receiver. *Acta Opt. Sin.* **2017**, *37*, 1222003.
31. Venegas-Reyes, E.; Martin-Dominguez, I.R.; Carrasco, U.D.; Enciso, R.A.P. Optical design and simulation of a circular trough solar concentrator with trapezoidal secondary reflector. In Proceedings of the 11th ISES Eurosun 2016 Conference, Palma, Spain, 11–14 October 2016; pp. 1136–1143.

32. Yang, Y.; Wei, Q.Y.; Hou, J.Y.; Liu, H.; Zhao, L. Solar concentrator with uniform irradiance for particulate photocatalytic hydrogen production system. *Int. J. Hydrogen Energy* **2016**, *41*, 16040–16047. [CrossRef]
33. Wei, Q.Y.; Yang, Y.; Liu, H.J.; Liu, M.C.; Cao, F.; Zhao, L. Experimental study on direct solar photocatalytic water splitting for hydrogen production using surface uniform concentrators. *Int. J. Hydrogen Energy* **2018**, *43*, 13745–13753.
34. Cao, F.; Li, Y.; Wang, L.; Zhu, T.Y. Thermal performance and stress analyses of the cavity receiver tube in the parabolic trough solar collector. *IOP Conf. Ser. Earth Environ. Sci.* **2016**, *40*, 012067. [CrossRef]
35. Wang, L.; Sun, J.; Zhang, Z.; Wei, J.J. A trans-dimensional multi-physics coupled analysis method for direct-steam-generation parabolic-trough loop. *Appl. Therm. Eng.* **2021**, *193*, 117011.
36. Zhang, C.Z.; Xu, G.Q.; Quan, Y.K.; Li, H.W.; Song, G. Optical sensitivity analysis of geometrical deformation on the parabolic trough solar collector with Monte Carlo Ray-Trace method. *Appl. Therm. Eng.* **2016**, *109*, 130–137. [CrossRef]
37. Duffie, J.A.; Beckman, W.A. *Solar Engineering of Thermal Process*, 3rd ed.; John Wiley & Sons, Inc.: New York, NY, USA, 2006; pp. 322–373.
38. Liu, T.; Wang, J.; Bing, Q.; Yang, F.; Feng, W.; Wang, D. Simulation study of concentrating characteristics of trough solar collector. *Acta Energy Sol. Sin.* **2017**, *38*, 3202–3209.
39. Cao, F.; Wei, Q.; Liu, H.; Lu, N.; Zhao, L.; Guo, L. Development of the direct solar photocatalytic water splitting system for hydrogen production in Northwest China: Design and evaluation of photoreactor. *Renew. Energy* **2018**, *121*, 153–163. [CrossRef]
40. Cao, F.; Liu, H.; Wei, Q.; Zhao, L.; Guo, L. Experimental study of direct solar photocatalytic water splitting for hydrogen production under natural circulation conditions. *Int. J. Hydrogen Energy* **2018**, *43*, 13727–13737. [CrossRef]